Motor neuron degeneration, severe myopathy and TDP-43 increase in a transgenic pig model of SOD1-linked familiar ALS

04 August 2020

Neurobiology of Disease 124 (2019) 263–275

Contents lists available at ScienceDirect

Neurobiology of Disease

journal homepage: www.elsevier.com/locate/ynbdi

Motor neuron degeneration, severe myopathy and TDP-43 increase in a transgenic pig model of SOD1-linked familiar ALS

Paola Crociara[a], Maria Novella Chieppa[a], Elena Vallino Costassa[a], Elena Berrone[a], Marina Gallo[a], Monica Lo Faro[a], Maria Domenica Pintore[a], Barbara Iulini[a], Antonio D'Angelo[b], Giovanni Perona[b], Alberto Botter[c], Donato Formicola[d], Alberto Rainoldi[d], Marianna Paulis[e,f], Paolo Vezzoni[e,f], Federica Meli[g], Fiorenzo Antonio Peverali[g], Caterina Bendotti[h], Maria Chiara Trolese[h], Laura Pasetto[h], Valentina Bonetto[h], Giovanna Lazzari[i,j], Roberto Duchi[i], Andrea Perota[i], Irina Lagutina[i], Corinne Quadalti[i], Maria Silvia Gennero[a], Daniela Dezzutto[a], Rosanna Desiato[a], Marina Boido[k], Matilde Ghibaudi[k], Maria Consuelo Valentini[l], Maria Caramelli[a], Cesare Galli[i,j], Cristina Casalone[a], Cristiano Corona[a,*]

[a] Istituto Zooprofilattico Sperimentale del Piemonte, Liguria e Valle d'Aosta, Via Bologna 148, 10154 Turin, TO, Italy
[b] Department of Veterinary Sciences, University of Turin, Largo Paolo Braccini 2, 10095 Grugliasco, TO, Italy
[c] Laboratorio di Ingegneria del Sistema Neuromuscolare (LISIN), Politecnico di Torino, Corso Castelfidardo 42/a, 10138 Turin, TO, Italy
[d] NeuroMuscularFunction research group, School of Exercise and Sport Sciences, Department of Medical Sciences, University of Turin, Piazza Gian Lorenzo Bernini, 12, 10143 Turin, TO, Italy
[e] Milan Unit, Istituto di Ricerca Genetica e Biomedica, CNR, Via Fantoli 16/15, 20138 Milan, MI, Italy
[f] Humanitas Clinical and Research Center, via Manzoni 56, 20089 Rozzano, MI, Italy
[g] Istituto di Genetica Molecolare, CNR, Via Abbiategrasso 207, 27100 Pavia, PV, Italy
[h] IRCCS-Istituto di Ricerche Farmacologiche "Mario Negri", Via La Masa, 19, 20156 Milano, MI, Italy
[i] Avantea, Via Porcellasco 7F, 26100 Cremona, CR, Italy
[j] Fondazione Avantea, Via Porcellasco 7F, 26100 Cremona, CR, Italy
[k] Neuroscience Institute Cavalieri Ottolenghi (NICO), University of Turin, Department of Neuroscience, Regione Gonzole 10, 10043 Orbassano, TO, Italy
[l] Department of Neuroradiology, A.O.U. Città della Salute e della Scienza, Corso Bramante 88, 10126 Turin, TO, Italy

ARTICLE INFO

Keywords:
SOD1
Transgenic pig
Amyotrophic lateral sclerosis
ALS
TDP-43

ABSTRACT

Amyotrophic Lateral Sclerosis (ALS) is a neural disorder gradually leading to paralysis of the whole body. Alterations in superoxide dismutase SOD1 gene have been linked with several variants of familial ALS. Here, we investigated a transgenic (Tg) cloned swine model expressing the human pathological hSOD1^{G93A} allele. As in patients, these Tg pigs transmitted the disease to the progeny with an autosomal dominant trait and showed ALS onset from about 27 months of age. Post mortem analysis revealed motor neuron (MN) degeneration, gliosis and hSOD1 protein aggregates in brainstem and spinal cord. Severe skeletal muscle pathology including necrosis and inflammation was observed at the end stage, as well. Remarkably, as in human patients, these Tg pigs showed a quite long presymptomatic phase in which gradually increasing amounts of TDP-43 were detected in peripheral blood mononuclear cells. Thus, this transgenic swine model opens the unique opportunity to investigate ALS biomarkers even before disease onset other than testing novel drugs and possible medical devices.

1. Introduction

Amyotrophic Lateral Sclerosis (ALS) is an adult-onset neurodegenerative disorder affecting both upper and lower motor neurons (MNs). Mutations in the gene coding for the antioxidant enzyme Cu, Zn-superoxide dismutase 1 (SOD1) occur in 10%–20% of familial ALS (FALS) cases and in up to 7% of sporadic ALS (SALS) cases (Andersen, 2006; Rosen, 1993). > 150 different mutations, mostly dominant inherited, have been identified in ALS patients. These findings enabled the subsequent development of novel experimental animal models: currently ALS research relies heavily on transgenic rodents expressing mutant human SOD1 (hSOD1). Accordingly, a MN disease phenotype results

* Corresponding author.
E-mail address: cristiano.corona@izsto.it (C. Corona).

https://doi.org/10.1016/j.nbd.2018.11.021
Received 20 March 2018; Received in revised form 26 October 2018; Accepted 19 November 2018
Available online 22 November 2018

from the expression of gain-of-function of different hSOD1 mutants in rodents, rather than SOD1 gene targeting (Turner and Talbot, 2008). These animal models contributed to the discovery of several pathogenetic mechanisms underlying the disease including axonal transport defects, oxidative stress, protein misfolding, mitochondrial dysfunction, excitotoxicity and altered RNA metabolism (Peviani et al., 2010), nevertheless the molecular mechanisms responsible for the selective MN degeneration are not yet fully elucidated. The lack of translation from bench to bedside represents a major drawback against this animal model (Benatar, 2007; Perrin, 2014). Several factors are supposed to be involved in the discrepancy between the results obtained in mouse models and patients including phylogenetic distance among species, size, lifespan and subtle differences of anatomical structures and physiology. Recent meta-analysis of drug trials in mice revealed that several studies were underpowered and most treatments were applied at pre-symptomatic stage, whereas treatments of ALS patients start only months or even years after the onset of the disease (Perrin, 2014). Interestingly, it has been suggested that the onset of clinical symptoms is preceded by a long pre-symptomatic period in which there is a system dysfunction but not clinical manifestations due to an intrinsic reserve within the neuromuscular system or recruitment of compensatory mechanisms (Eisen, 2014; Talbot, 2014). Understanding what happen during the long time elapsed between the onset of the pathological process triggered by the gene mutation and the onset of overt symptomatic disease has important implications as this phase is likely to be the best target for therapeutic trials. A critical issue is developing an ALS animal model which recapitulate the long preclinical/clinical phases as in patients, to allow the identification and validation of pre-symptomatic diagnostic biomarkers and biotargets for effective therapeutic interventions. In this respect, pigs which have a long lifespan and have been employed for modeling several human diseases including neurodegenerative disorders (Holm et al., 2016; Lind et al., 2007) may present advantages as compared to rodent models. As such, a hSOD1^{G93A} transgenic (Tg) swine was generated by somatic cell nuclear transfer (SCNT) of primary porcine adult male fibroblasts stably expressing the pathological allele of the human SOD1 gene carrying the glycine-to-alanine conversion at the 93rd codon (G93A) (Chieppa et al., 2014).

Here, we showed that hSOD1^{G93A} Tg swine shares several features of ALS at the symptomatic phase. Moreover, the disease is transmissible to the progeny with mendelian traits. Contrary to the rodent models, these Tg pigs have a quite long pre-symptomatic phase of about 27 months of age, which is a relevant pathological feature in common with patients.

Furthermore, we investigated TDP-43, a major neuropathological hallmark of ALS (Neumann, 2009). In spinal cord of ALS patients, TDP-43 pathology is most commonly observed in sporadic cases, but it has also been detected in mutant-SOD1 familial cases and mouse models (Lauranzano et al., 2015; Marino et al., 2015; Sumi et al., 2009). Increasing amounts of the total TDP-43, which parallel disease progression, were found in peripheral blood mononuclear cells (PBMCs) of sporadic ALS patients (Filareti et al., 2017; Nardo et al., 2011). Accordingly, a progressive TDP-43 raise was also observed in PBMCs of hSOD1^{G93A} Tg swine before the onset of the symptomatic phase. All together these findings suggest that the hSOD1^{G93A} Tg pigs represent a remarkable ALS model and may strongly contribute to further support clinical research of ALS.

2. Materials and methods

2.1. Animals and breeding

All procedures were conducted as described by the institutional guidelines that are in accordance with national (D.L. no. 116, G.U. suppl. 40, February 18, 1992, no. 8, G.U., 14 luglio 1994; D.L.26/2014) and international laws and policies (EEC Council Directive 86/609, 63/2010, OJ L 358, December 12, 1987; National Institutes of Health Guide for the Care and Use of Laboratory Animals, US National Research Council, 1996). hSOD1^{G93A} Tg pigs were produced as previously reported (Chieppa et al., 2014). Among the four Tg cloned founder pigs (168, 174, 204, 205) that reached adulthood, Tg 168 was bred to establish a transgenic line and Tg 168 progeny was further investigated. The specific number of animals or samples used was stated in the figure captions. All experiments were designed to minimize the number of animals used and their discomfort (project authorization n 1043/2016-PR from Ministry of Health).

2.2. qPCR

To determine the transgene copy number the $2^{-\Delta\Delta ct}$ method was applied, using genomic human DNA as a calibrator. The qPCR was performed using the iTaq Universal Sybr Green Supermix (Bio-Rad) and the following primers pair: SOD1Fw (5′-catgaacatggaatccatgcagg-3′) and SOD1Rw (5′-taatggaccagtgaaggtgtg-3′) for the human SOD1 gene and gapdhFW (5′-tgccacccagaagactgtgg-3′) and gapdhRW (5′-accttgcccacagccttggc-3′) for the glyceraldehyde-3-phosphate dehydrogenase as housekeeping gene. The program set on a Mx3000P thermocycler (Stratagene) consists of forty cycles composed of a denaturation step at 95 °C for 10 s followed by an annealing/extension step at 62 °C for 30 s. Data were presented as delta cycle threshold (ΔCt) between the SOD1 and housekeeping gene. The ΔCt values in Tg pigs and calibrator DNA were converted to relative transgene copy number by the equation $2^{-\Delta\Delta Ct}$.

2.3. RT-PCR

To determine MCP-1 mRNA levels total RNA was extracted from cervical spinal cord using the Trizol method (Invitrogen) and purified with PureLink RNA columns (Thermo Fisher Scientific). Real-time PCR was performed using the Taq Man Gene expression assay (Applied Biosystems) following the manufacturer's instructions, on 50 ng of cDNA specimens in triplicate, using 1× Universal PCR master mix (Thermo Fisher Scientific) and 1× mix containing the specific porcine probe for MCP1 (Ss03394377_m1; Thermo Fisher Scientific). Relative quantification was calculated from the ratio between the cycle number (Ct) at which the signal crossed a threshold set within the logarithmic phase of MCP1 gene and that of the reference β-actin gene (Ss03376081_u1; Thermo Fisher Scientific). Mean values of the triplicate results for each animal were used as individual data for $2^{-\Delta\Delta Ct}$ analysis.

2.4. Fluorescent in situ hybridization (FISH)

FISH experiments were carried out as previously described on interphase and metaphase cells from three Tg founder pigs (168, 174, 204) (Paulis et al., 2015). Tg 205 was not analyzed since it was a Tg 204-clone. Briefly, cell cultures were treated with KaryoMAX colcemid (Thermo Fisher Scientific) at a final concentration of 0.1 μg/ml for 2 h at 37 °C and cells were then detached by treatment with 0.25% trypsin/EDTA (Lonza). After hypotonic treatment with 0.075 M KCl and fixation in methanol: acetic acid (3:1 v/v), the cell suspension was dropped onto a slide and air dried. Slides were treated with 0.004% Pepsin (Sigma Aldrich) at 37 °C for 10 s and dehydrated through the ethanol series before denaturation in 70% formamide/2xSSC. The hSOD1^{G93A} DNA vector was used as DNA probe. The DNA was labeled via nick translation (Enzo Life Sciences), using Bio-11-dUTP (Roche Diagnostics) and resuspended in hybridization buffer (50% formamide, 10% dextran sulphate, 1× Denhart's solution, 0.1% SDS, 40 mM Na2HPO4 pH 6.8, 2xSSC) containing 10× Salmon Sperm DNA. Before hybridization the probes were denatured at 80 °C for 10 min and pre-annealed at 37 °C for 20 min. Hybridization was carried out overnight at 37 °C. Stringent washings were performed in 50% formamide/2xSSC at 42 °C. For biotin

detection, the slides were incubated with FITC-conjugated avidin DCS (Vector Laboratories), then with biotin-conjugated anti avidin D antibody (Vector Laboratories) and finally with FITC-conjugated avidin DCS. Avidin and all the antibodies were used at a final concentration of 5 μg/ml. Slides were mounted in Vectashield mounting medium with DAPI (Vector Laboratories), and then were scored under an Olympus BX61 Research Microscope equipped with a cooled CCD camera. Images were captured and analyzed with Applied Imaging Software CytoVision (CytoVision Master System with Karyotyping & FISH). To identify individual chromosomes and to assign the location of signals to specific chromosome regions, inverted digital images of DAPI banded chromosomes were used. For each sample at least 20 metaphases and 100 interphase nuclei were analyzed.

2.5. Splinkerette assay

The splinkerette ligation-mediated PCR was applied, as described in (Potter and Luo, 2010). Briefly, the oligonucleotides *SPLNK-BOT2* (5′- cga agagtaaccgttgctaggagagaccgtggctgaatgagactggtgtcgacactagtgg -3′) and *SPLNK-AATT-ApoI* (5′-aattccactagtgtcgacaccagtctctaatttttttttttcaaaaaaa-3′) were annealed to generate the *Apo*I splinkerette linker. In parallel, genomic DNA (gDNA) of the Tg 168 founder was purified with standard procedure based on sodium dodecyl sulphate lysis supplemented with proteinase K followed by rounds of phenol and chloroform extractions. Purified gDNA was then *Apo*I digested and an aliquot (about 200 ng) was ligated with a 10-fold molar excess *Apo*I-splinkerette linker in a volume of about 50 μl. Ligated DNA was then amplified by three rounds of nested-PCR with *v3-F1* (5′- cattaattgcgttgcgctcactgc-3′), *v3-F2* (5′- ggtttgcgtattgggcgctcttc-3′) and *v3-F2* (5′- ggtttgcgtattgggcgctcttc-3′) outward primers targeting the 3′ end of the integrated vector and the *SPL-S1* (5′- cgaagagtaaccgttgctaggagagacc-3′) and *SPL-S2* (5′- gtggctgaatgagactggtgtcgac-3′) primers targeting the *Apo*I-splinkerette linker. The chimeric plasmidic-genomic amplified DNA was then sequenced by standard procedure. Next, undigested Tg 168 gDNA template was amplified with the *v3-F1*, *v3-F2* and *v3-F3* outward primers together with the *g3-R1* (5′-ctccagtctcttacttcacccaactc-3′), *g3-R2* (5′- gcatcttcttagtctcagagcctcaaacc-3′) and *g3-R3* (5′gataaatgttctcctgcacctattaatg-3′) to prove that the vector is indeed contiguous with the isolated 3′ flanking sequence. The primers targeting the 3′-flanking sequence gDNA, *g3-R1*, *g3-R2* and *g3-R3* were also coupled with the *g5-F1* (5′- ggaattaggagggtttggaaatagaactc-3′), *g5-F2* (5′- ggatagtcagcacatgcaacactgcattc-3′) and *g5-F3* (5′- gaggatcactggtttaa-tagggtgtagag-3′) primers targeting the 5′ flanking sequence of the genomic breakpoint to demonstrate that only one sister chromosome 2 was targeted by the tandem integration of the vectors into the Tg 168 genome.

2.6. Neurological examination

Neurologic examination was performed monthly by a veterinary neurologist. An examination protocol was properly developed and adapted to the pigs and followed the standard procedure for assessing mental status, posture, gait, postural reactions and proprioception, cranial nerves, spinal reflexes and sensitivity.

2.7. Motor function analysis

Pigs underwent a qualitative and quantitative digital gait analysis (3D Motion Capture system, 3DMC), using a 3D computerized system with 2 cameras. A stereoscopic video system was used to analyze the qualitative biomechanics of the pig gait strategy. The two camcorders were placed on two tripods with a height of 50 cm from the ground and with a parallelism between the focal axes. The binocular vision system was designed to record 10 m panoramic field of view. An audio trigger system was used to synchronize the camcorders. Surface electromyography (sEMG) signals were detected from gastrocnemius and tibialis anterior simultaneously with video recordings. For each muscle, myoelectric activity was recorded in bipolar configuration with a pair of surface electrodes (1.2 cm^2, 3 cm inter-electrode distance; Kendall) positioned over the muscle belly. Prior to electrode positioning the skin region was shaved, abraded and cleaned with alcohol to improve the mechanical and electrical stability of the electrode-skin contact. The synchronization between sEMG signals and videos was ensured by a custom-made video trigger. This device was positioned in the field of view of the camera. The video trigger generates a flashing light in correspondence of the start and the end of sEMG acquisition. The video frames corresponding to the beginning and the end of the sEMG acquisition can be identified, thus allowing the offline re-alignment of sEMG and video recordings. The motor function protocol consisted in a set of gait tasks. The animal was free to walk in a linear trajectory along a 5 m asphalted sidewalk. When the pig arrived to the finish of the sidewalk, it turned around and came back to start a new gait cycle. Gait tasks were recorded, in a forward direction and in a return direction. A specialized operator controlled the direction of the gait and assisted the animal during the turning phase with a manual bulkhead. Video and sEMG signals were analyzed using a custom-written software in Matlab (R2016a, The MathWorks Inc.). Raw sEMG signals were bandpass filtered (30 Hz to 500 Hz, 4th order non-causal Butterworth filter). EMG envelopes were obtained by full-wave rectification and low pass filtering (cutoff frequency = 5 Hz, 2nd order non-causal Butterworth filter) of raw EMGs. EMG envelopes of individual muscles were segmented in time in N epochs corresponding to the duration of the gait cycle. The gait cycle was defined as the time interval between two successive contacts of the right-posterior paw. Ground contacts of each paw were visually assessed by the investigators with an accuracy of ± 1 video frame (i.e. 40 ms, being 25 Hz the frame rate of the camera). Segmented sEMG epochs were normalized in time by interpolating data points over a time base of 1000 points for each gait cycle (Courtine et al., 2005) and by fitting the data with a cubic spline to (Thorup et al., 2008). Eventually, the obtained profiles of sEMG activity during the normalized gait cycle were averaged for each muscle.

2.8. Histology and immunohistochemistry

Pigs were sacrificed according to the approved protocol of animal welfare. Brain and spinal cord were rapidly dissected out and formalin immersion-fixed for histology/immunohistochemistry or 4% PFA immersion-fixed for immunofluorescence analysis. Tissues were then paraffin embedded or crioprotected in 30% sucrose and OCT embedded, respectively. For histological analysis 5 μm sections were stained with hematoxylin and eosin (H&E). Immunostaining was performed with the following antibodies: anti Golgi Complex (1: 50, Abcam, ab103439), anti GFAP (1: 100, Millipore, MAB 3402), anti Iba1 (1: 600, Biocare, CP290A), anti Cleaved Caspase-3 (1: 150, Cell Signaling Technology, 9661), anti Microtubule associated proteins 1A/1B light chain 3, LC3 (1:200, Sigma-Aldrich, L8918), anti human SOD1 (1: 600, Abcam, ab 79,390), anti SOD1 exposed dimer interface [(SEDI), 1: 700, StressMarq Bioscineces Inc., SPC-206P], anti Neurofilament H non-phosphorylated SMI 32 (1: 1000, Bio Legend, SMI-32R), anti-Neurofilaments, phosphorylated SMI 31 (1: 5000, Bio Legend, SMI-31R), anti peripherin (1: 1000, Millipore, AB 1530), anti TDP-43 (1: 1000, Proteintech, 10,782–2-AP), anti phospho TDP-43 (1: 1000, Cosmo Bio Co., Ltd., TIP-PTD-P02). For DAB staining, sections were incubated 1 h at RT with biotinylated goat-anti-mouse/rabbit (Vector Laboratories) followed by ABC reagents (Vector Laboratories) and developed with DAB reagent (Sigma Aldrich). For immunofluorescence staining, sections were incubated with Alexa Fluor -conjugated secondary antibodies (1: 1000, Thermo Fischer Scientific) for 1 h at RT and counterstained with DAPI (1: 1000, KPL, 71–03-01). For the terminal deoxynucleotidyl transferase dUTP nick end labeling (TUNEL) assay, the DeadEnd Colorimetric TUNEL System Kit (Promega) was used according to the manufacturer's protocol.

Biopsy tissue obtained from several muscles was precooled in

isopentane and frozen in liquid nitrogen. Frozen muscle cross sections of 8 μm thickness were produced and routine histological and enzyme activity analyses of the sections were conducted: H&E, Gomori trichrome (MGT), periodic acid Schiff staining (PAS), succinate dehydrogenase (SDH), nicotinamide adenine dinucleotide tetrazolium reductase (NADH-TR), cytochrome oxidase (COX), and adenosine triphosphatase (ATPase).

2.9. Motor neuron analyses

For MNs quantification, a series of one-in-ten sections (50 μm apart) through different levels of the entire spinal cord, for each animal was analyzed. At least 6 Cresyl violet (CV) stained sections per spinal cord level were analyzed. Only neurons with a mean diameter ≥25 μm and prominent nuclei and nucleoli and located in the anterior horn of the spinal cord, were counted using a 40× objective under a light microscope (Leica Microsystems). For the count of LC3-positive puncta visible into the MN soma, the samples were observed with a Leica TCS SP5 confocal laser scanning microscope (Leica Microsystems) to create 3D reconstructions. Confocal stacks were analyzed by Image J software: at least 80 MNs were evaluated and LC3-positive puncta visible into the MN cell body were counted.

2.10. Neuromuscular junction (NMJs) analysis

Gastrocnemius and peroneus muscles were immersion-fixed in 4% PFA for 48 h, cryoprotected in 30% sucrose and sectioned at 40 μm thickness on a freezing microtome. NMJs were visualized using Alexa 555-conjugated α-bungarotoxin (BTX, 1: 1000, Thermo Fisher Scientific) to label post-synaptic acetylcholine receptors and Neurofilament (1: 50, Novocastra, NCL-l-NF200-N52) to bind MN axons. Endplates were considered innervated if there was a complete overlay with the axon or denervated if the endplate was not occupied by MN terminal axons. In case of partial overlap, the NMJs were considered as partially innervated. At least 100 randomly selected endplates per muscle were analyzed using an epifluorescence microscope (Nikon).

2.11. Electron microscopy

Tg and control (CTR) lumbar spinal cord segments, gastrocnemius muscle and sciatic nerve specimens were fixed by immersion in a solution containing 2.5% glutaraldehyde and 0.5% sucrose in 0.1 M Sorensen phosphate buffer, until embedding. Samples were then post-fixed in 1% osmium tetroxide and dehydrated in ascending series of ethanol (from 30% to 100%). After two brief passages in propylene oxide and o/n in a mixture of propylene oxide and Glauerts mixture of resins, specimens were embedded in Glauerts mixture of resins (50:50 Araldite M and Araldite Harter, HY 964): in the resin mixture, 0.5% of the plasticizer dibutylphthalate was added, followed by 2% of accelerator 964, used to promote the polymerization of the embedding mixture. Semi-thin (1-μm thick) sections were then cut, using a Ultracut UCT ultramicrotome (Leica Microsystems) and stained by 1% Toluidine blue for light microscopy examination and morphological analysis. For transmission electron microscopy (TEM), ultra-thin sections (80-nm thick) were cut using the Ultracut UCT ultramicrotome, and counterstained with Uranyl Acetate Replacement Stain (Electron Microscopy Sciences). Ultra-thin sections were observed by a JEM-1010 TEM (JEOL) equipped with a Mega-View-III digital camera and a Soft-Imaging-System (SIS). Sciatic nerve samples were also examined for morphological analysis. For the g-ratio measurement (i.e. ratio of the inner axonal diameter to the total outer diameter), toluidine blue stained sections of Tg and CTR sciatic nerve were analyzed: approximately 150 axons have been evaluated for each group. Fiber (i.e. axon and myelin) and axon diameters have been measured by Neurolucida software (MicroBrightField), using the “quick measure line” tool.

2.12. Western blotting

Protein extracts were prepared from central nervous system -CNS- (spinal cord, brainstem, cerebellum, cortex and striatum) and muscles homogenates. Depending on the experimental reasons to be achieved, different extraction protocols have been used. We analyzed either soluble and/or triton insoluble fractions (TIF) according to (Ouyang and Hu, 2001).

Western blotting was performed using SDS polyacrylamide gels (NuPAGE 4–12% Bis-Tris gel or 12% Bis-Tris gel, Invitrogen) with 25 μg of protein extract loaded per lane. PVDF membranes (Bio-Rad) were incubated with primary antibodies raised against SOD1 (1:1000, Abcam 79,390; 1:500, Sigma Aldrich, HPA0014101), GFAP (1:1000, Millipore MAB3402), Iba1 (1:100, Millipore MABN92) overnight at 4 °C, followed by peroxidase-conjugated secondary antibodies. Gels were stripped and reprobed with anti GADPH (1: 1000, Santa Cruz sc-166,574). Signals were acquired with the ChemiDoc™ Touch Gel Imaging System.

2.13. PBMC isolation and protein extraction

PBMCs were isolated from pigs peripheral venous blood essentially as previously described (Nardo et al., 2011). Briefly, samples of blood were collected in EDTA pre-coated tubes (BD Vacutainer® K2EDTA) and PBMCs were isolated from EDTA blood by Ficoll-Hypaque (Ficoll-Plaque™ Plus, GE Healthcare) density gradient centrifugation at 800 ×*g* for 30 min at 18–20 °C. Mononuclear cells were collected from the interface and washed three times with RPMI 1640 medium (EuroClone). Platelets were eliminated by an additional wash and centrifugation at 200 ×*g* for 10 min. PBMCs were stored as pellets at −80 °C. Before analysis, PBMCs were lysed in 20 mM Tris-HCl pH 7.5, 0.1% NP40 and 0.1% SDS supplemented with Protease Inhibitors (Sigma) and incubated at 95 °C for 5 min. Samples were centrifuged at 16.000 ×*g* for 10 min at 4 °C and protein concentration in supernatants was analyzed by the BCA protein assay (Pierce). Supernatants were analyzed by dot blot analysis.

2.14. TDP-43 pathology by biochemical approaches

To evaluate TDP-43 aggregation, TIF was isolated from frontal cortex and spinal cord tissues of Tg and control pigs and analyzed by dot blot, as described (Basso et al., 2009).

To evaluate TDP-43 mislocalization in cervical spinal cord of the Tg 168 pig, TDP-43 level was measured in the nuclear and cytoplasmic fractions in comparison with a control animal (CTR1). Subcellular fractionation of the tissue was done as previously described (Lauranzano et al., 2015; Pasetto et al., 2017). Mouse monoclonal anti-GAPDH (1:10.000 dilution; Millipore) and mouse monoclonal anti-lamin A/C (1:500 dilution; Chemicon) were used, respectively, as cytoplasmic and nuclear markers. Level of TDP-43 in nuclear and cytoplasmic fractions was analyzed by dot blot.

2.15. Dot blot analysis

Protein lysates (3 μg) from PBMC, nuclear and cytoplasmic fractions and TIF were directly loaded onto nitrocellulose Trans-Blot transfer membranes (Bio-Rad) by vacuum filtration, as described previously (Nardo et al., 2011). An internal standard which is a pool of all samples in the analysis was deposited in triplicates. Dot blot membranes were blocked with 3% (*w/v*) BSA (Sigma Aldrich) and 0.1% (v/v) Tween 20 in Tris-buffered saline, pH 7.5, incubated with rabbit polyclonal anti-TDP-43 primary antibody (1:2500 dilution; Proteintech), then with anti-rabbit peroxidase-conjugated secondary antibody (1:5000 for IB; Santa Cruz Biotechnology Inc.). Blots were developed with Luminata™ Forte Western Chemiluminescent HRP Substrate (Millipore) on the ChemiDoc XRS system (Bio-Rad). Densitometry was done with Progenesis PG240 v2006 software (Nonlinear Dynamics). The

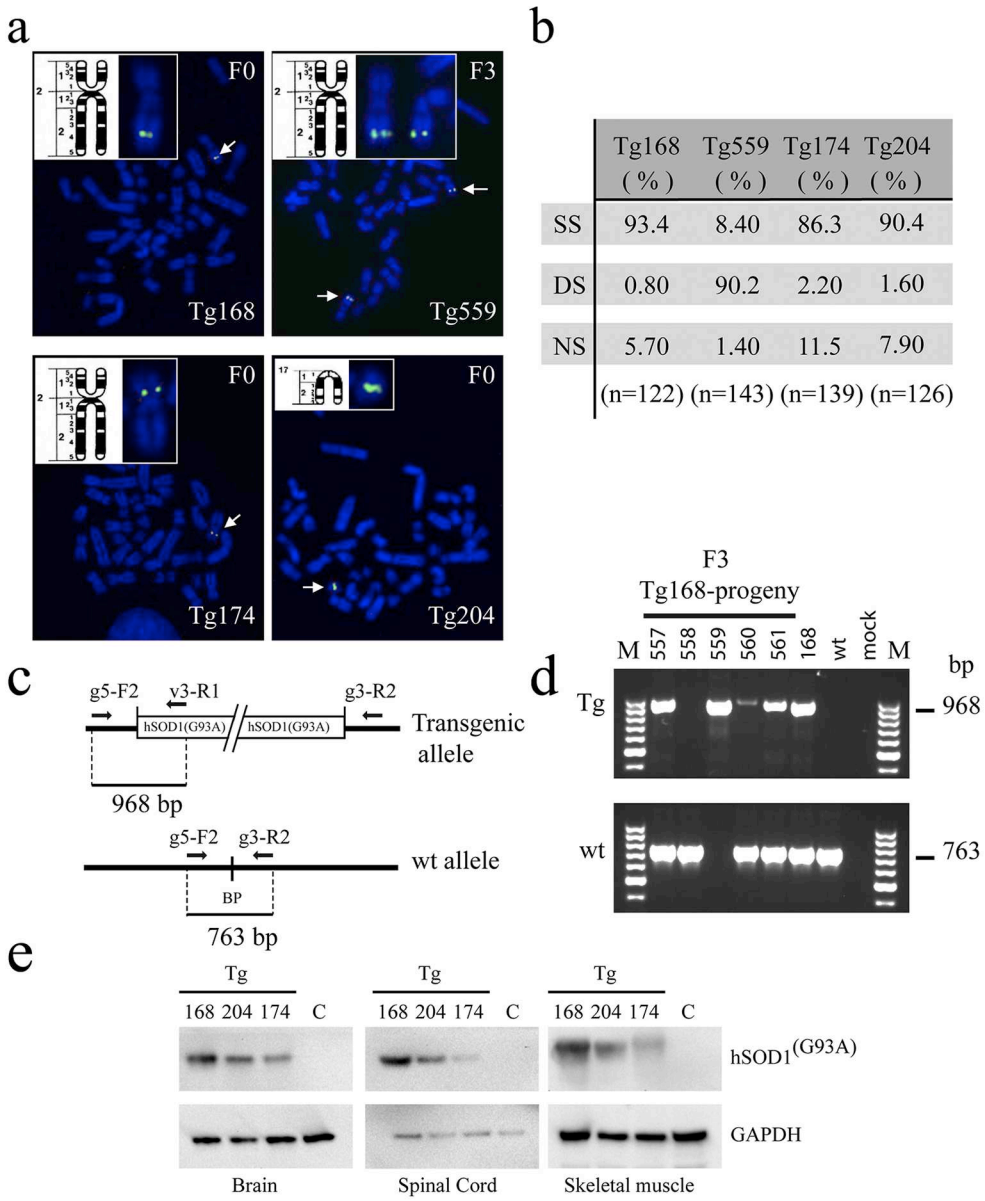

Fig. 1. Molecular characterization of hSOD1^{G93A} Tg pigs. (a) FISH analysis on metaphase spreads obtained from fibroblasts of three hemizygous founders (Tg 168, 174 and 204) and one F3 homozygous Tg168-progeny (Tg 559) using the hSOD1^{G93A} plasmid as probe (green). Inserts show the chromosome ideogram and the respective enlarged section of the metaphase with the hybridized chromosome. Chromosomes were counterstained with DAPI (blue); white arrows indicate the localization of the probe. (b) Interphase FISH analysis on nuclei obtained from fibroblasts. The percentage of the number of signal/nucleus is indicated. SS: Single Signal; DS: Double Signals; NS: No Signal. n indicates the number of nuclei counted. (c) Schematic representation of the PCR assay used for genotyping the Tg 168 pig and its progeny (see also Fig. S1). The (g5-F2; v3-R1) primer set amplifies the 968 bp band of the transgenic allele, whereas the (g5-F2; g3-R2) primer set amplifies the 763 bp band of the endogenous wild type allele. (d) Representative TBE-agarose gel electrophoresis of the PCR products, as described in c, on gDNAs extracted from third generation (F3) pigs of the Tg 168-progeny (see also legends of Fig. 2 and Fig. S1). (e) The abundance of hSOD1 is compared to GAPDH by immunoblot of samples isolated from brain, lumbar spinal cord and skeletal muscle of hSOD1^{G93A} Tg cloned founder boars. C: control. (For interpretation of the references to colour in this figure legend, the reader is referred to the web version of this article.)

immunoreactivity of the different proteins was normalized to Ponceau Red staining (Fluka) and to the internal standard of each membrane.

2.16. Statistical analysis

Statistical data analysis was performed using STATA 14 (Stata Corp, College Station, TX) and GraphPad Prism 5 software (La Jolla). It was performed a univariate analysis based on multilevel mixed-effects linear regression models for immunoblot analysis (hSOD1, GFAP, Iba1), MNs count and NMJs analysis, a Kolmogorov- Smirnov test for sEMG, a Mann Whitney *U* test for 3DMC, an unpaired *t*-test for LC3-positive puncta count, g-ratio, fiber size and myelin thickness measurements, a chi square test for fiber size distribution analysis and a one-way ANOVA with Tukey's multiple comparisons test for TDP-43 levels, as specified in the figure legends. $P < .05$ was considered significant.

3. Results

3.1. Molecular analysis of cloned hSOD1^{G93A} Tg pigs

Transgenic cloned founder pigs expressing the human pathological allele hSOD1^{G93A} were previously generated by SCNT of primary porcine fibroblasts and the transgene integration pattern of the *Apa*L1 linearized pMG5 ′ 3′ MARPuro-hSOD1 G93A plasmid vector analyzed by Southern blot (Chieppa et al., 2014). Here, cytogenetic mapping was carried out by fluorescent in situ hybridization (FISH) on interphase and metaphase chromosomes of primary fibroblasts isolated from Tg 168, Tg 174, Tg 204 cloned founder pigs and a third generation (F3) Tg168-progeny, Tg 559 pig. Single multiple transgene copies (see below) were integrated in single genomic sites mapped on 2q24 (Tg 168), 2p11 (Tg 174) and 17q21 (Tg 204), whereas the Tg168-F3 progeny, Tg 559, showed integration of the transgenic DNA on 2q24 band of both sister chromosomes, respectively (Fig. 1a, b). By quantitative PCR, about 20 copies of the hSOD1^{G93A} transgene were estimated to be integrated in tandem in the genomic site of the Tg 168 founder, whereas about 5 copies for Tg 204 pig and even a lower copy number for Tg 174. Since the onset of the disease was clearly evident at 27 months of age in the Tg 168 founder and the disease transmitted to the progeny (Fig. 2d), the Tg 168 transgenic line was further investigated by splinkerette ligation-mediated PCR to map at high resolution the genomic integration site (Fig. S1a-c).

A chimeric PCR fragment of about 700 bp was amplified from the 3′-

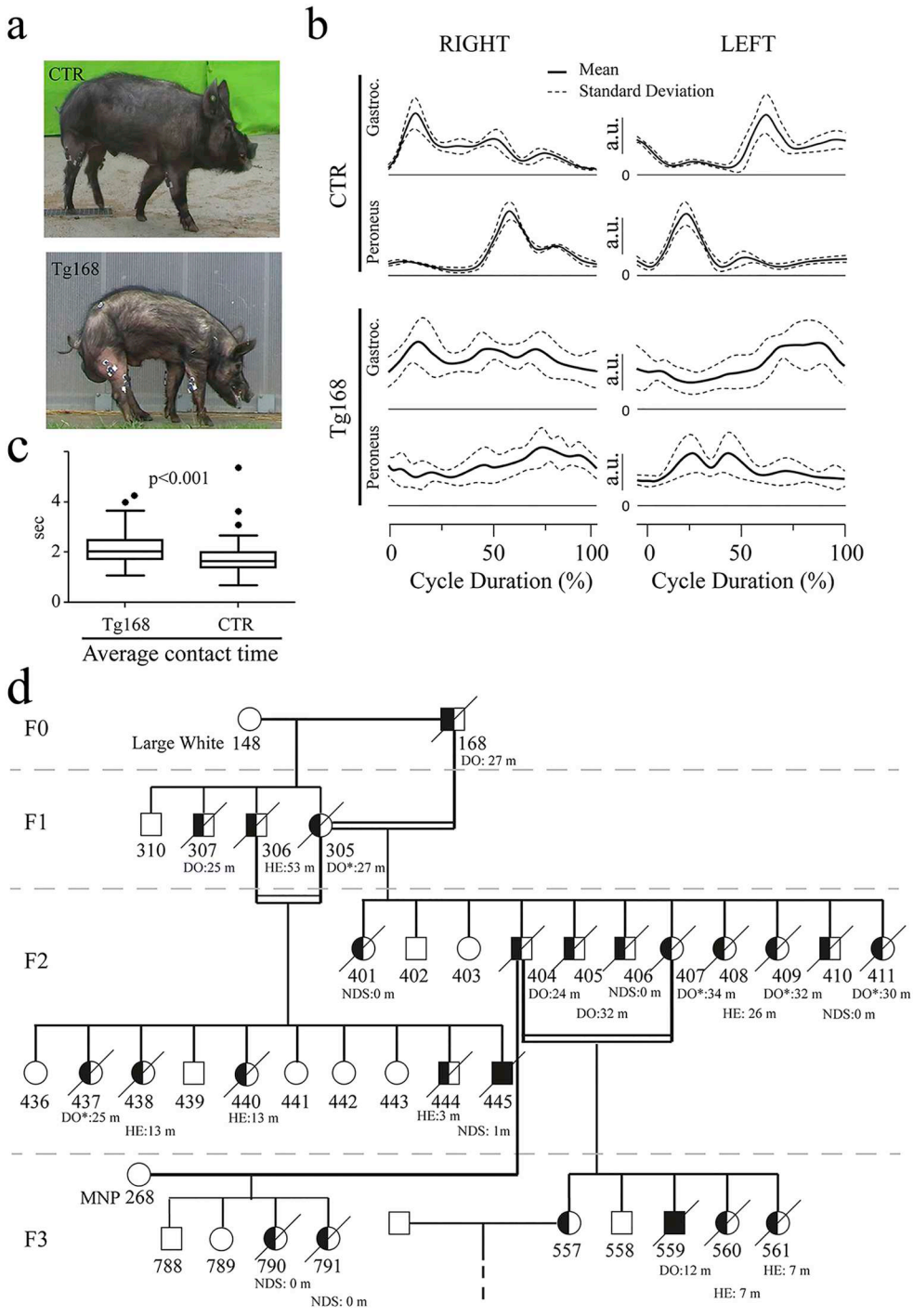

Fig. 2. Phenotype of hSOD1^{G93A} Tg pigs. (a) Representative image of CTR and Tg 168 at the end point (31 months old) with hindlimb spastic paralysis. (b) Time courses of the EMG signal envelopes in CTR and Tg 168 symptomatic pigs. A gait pattern alteration (in shape and variability) is clearly recognized in Tg 168 in both muscles for both sides (Kolmogorov-Smirnov test, $P < .001$). (c) Differences in average contact time between CTR and symptomatic Tg 168 pigs (Mann Whitney *U* test, $P < .001$, Tukey representation). (d) Family tree of transgenic line obtained from Tg 168 founder showing that the transgene and the ALS-like phenotype are inherited in an autosomal dominant fashion. In the diagram females are represented by circles and males are represented by squares. A half black-shaded symbol indicates that pig inherited the hSOD1^{G93A} transgenes in hemizygosis, whereas full black shaded symbol in homozygosis; Open symbols are wild type pigs. A slashed symbol indicates that pig was euthanized or died suddenly. DO (months): disease onset associated to motor deficits or to a labored breathing; DO* (months): indicates sudden death due to acute respiratory failure after sedation; HE: Euthanasia on Health (months) indicate pigs which were sacrificed before overt clinical symptoms; NDS: not determined sickness (months) are pigs died for causes other than disease or euthanized soon after birth.

end of the integrated vector joined to one of the flanking sequences of the host genome. BLAST alignment revealed that the bp 1–309 segment of the chimeric sequence shared 100% identity with the 3'end of the vector, the bp 310–669 segment was 99.72% aligned on chromosome 2 with the *Sus scrofa* 11.1 chr2:124045533-124045892 (Ensembl release 91) (Reference Sequence NC_010444.4: bp124045533-124045892) genomic sequence and the bp 666-674 segment shared 100% identity with the sequence of the *Apo*I-splinkerette linker.

Further PCR assays on undigested Tg 168 gDNA allowed to precisely map at 124045533 bp the genomic breakpoint on one of the two sister chromosomes 2 (hemizygosity) of Tg 168 and to show that the two most external copies of the tandem repeats of the vector were in opposite orientation.

Importantly, the integration site of Tg 168 was mapped quite far from known coding genes about 655 kb from the FAM170A-like gene at the 5'end and about 288 kb from the proline-rich protein 16 gene at the 3'-end, supporting the evidence that no coding genes were interrupted by the integration event. In addition, genotype analysis of the Tg 168 progeny confirmed that the ALS disease was always associated with the presence of integrated array of the hSOD1^{G93A} transgenes and that the disease was transmitted to the progeny as a dominant autosomal mendelian trait (Figs. 1c, d and 2d). Moreover, the copy number was stable within subsequent Tg 168 generations corresponding to about 20 copies in heterozygous pigs while homozygous pig (Tg 559) carrying twice the number of copies as do heterozygous pigs.

Immunoblot analysis revealed that the amounts of the transgenic hSOD1^{G93A} protein in Tg 168 extracts of the brain, spinal cord and muscles were significantly higher compared with parallel tissue samples harvested by the Tg 174, Tg 204 founder pigs. The hSOD1^{G93A} abundance in the Tg 168 tissues was estimated about 6-fold higher compared with Tg 174 tissues (Fig. 1e). Lastly, the mutant hSOD1 protein amounts in the brain and spinal cord were comparable among the different Tg 168 progeny (F1, F2 and F3; Fig. S8).

3.2. A dominant autosomal trait of ALS-like phenotype is shown in hSOD1^{G93A} Tg 168 swine family

Cloned hSOD1^{G93A} Tg founder pigs developed normally with respect to posture, gait and behavior and they reached adulthood. At 27th months of age, Tg 168 founder boar, carrying multiple copies of the transgene (≤ 20 copies) and the highest transgene expression levels, started to show gait abnormalities. The initial clinical manifestations were an unilateral hind limb lameness and a reduction in spontaneous walking activity in the cage. At 28 months of age, Tg 168 developed moderate ataxia and hypermetria of hind limbs. At 29–30 months of age the neurologic phenotype progressively worsened, involving also the front limbs and consisting in prolonged lateral recumbency and cough during eating. At 31 months of age Tg pig showed trembling when standing, severe ataxia, spastic tetraparesis more pronounced on hind limbs and dyspnea (Fig. 2a; Video S1, S2). This stage was established as humane end point and therefore the Tg 168 pig was euthanised and deeply investigated. By contrast, no further post mortem investigations were carried out on Tg founders, Tg 174, Tg 204 and Tg 205 (Tg 204-clone), that did not show any clinical signs of disease up to 5 years, likely due to insufficient amount of exogenous hSOD1^{G93A} protein to trigger the phenotype. Surface EMG (sEMG) time courses during the gait cycle for gastrocnemius and peroneus muscles of symptomatic Tg 168, asymptomatic Tg founder pigs (Tg 174, Tg 204, Tg 205) and an age matched non transgenic CTR pig were performed. Qualitative and quantitative assessment between EMG traces of the Tg 168 and CTR pigs revealed significant differences ($P < .001$) suggesting a clear alteration of the gait pattern in both muscles bilaterally (Fig. 2b). Electrophysiological analysis by sEMG exhibited a clear pattern of co-contraction of the gastrocnemius and peroneus muscles in Tg 168 pig at the end stage but not in CTR pig or other asymptomatic Tg pigs. As expected, 3DMC analysis, showed that the average ground contact time of the symptomatic Tg 168 was found greater than the CTR, to confirm altered gait (CTR: 1.78 ± 0.07 s vs Tg 168: 2.15 ± 0.07 s; $P < .001$; Fig. 2c). Analogous clinical features were observed in Tg 168 progeny, the F1 (Tg 307), the F2 (Tg 404, Tg 405), and the F3 (Tg 559) pigs. Interestingly, the onset of disease in homozygous Tg animal (Tg 559) was earlier (12 months) than in hemyzygous pigs (27 months) (Fig. 2d). Moreover, a subset of hemizygous Tg pigs (Tg 305, Tg 407, Tg 409, Tg 411, Tg 437) showed a labored breathing caused by respiratory muscle weakness and a sudden death due to an acute respiratory failure (ARF) during sedation for some clinical procedures, even in the absence of overt motor deficits (Fig. 2d).

3.3. ALS neuropathological features are evident in hSOD1^{G93A} Tg pigs

In end-stage Tg symptomatic pigs (Tg 168 and progeny), H&E and CV staining of spinal cord sections showed MN shrinkage and atrophy. By analyzing the semi-thin sections of Tg lumbar spinal cord, several degenerating, condensed MNs were observed compared to CTR pig (Fig. 3a, b). MNs exhibited darkened and shrunken cytoplasm, with crenated cell membrane, consistent with degeneration (Fig. 3b). Electron microscopy images also revealed evident nuclear alterations, characterized by presence of nucleolar cavities and electron dense granules in Tg pig with respect to CTR pig (Fig. 3c, d). Moreover, immunostaining examination of MN Golgi apparatus (GA), revealed fragmentation and reduced GA content in Tg compared to CTR pigs (Fig. 3e, f). Quantification of CV-stained spinal cord MNs revealed a statistically significant decrease of MN counts at cervical and thoracic (C1-C2, T6-T8, T9-T11) levels in Tg pigs (Fig. 3g). Average differences of MN counts in Tg pigs compared with CTR group were 52% in C1-C2 ($P = .004$; 95% CI 17–88%), 43% in T6-T8 ($P = .017$; 95% CI 8–80%) and 42% in T9-T11 ($P = .037$; 95% CI 2.4–81%). A neuroinflammatory response was observed; in end stage Tg pigs lumbar spinal cord, Iba1 and GFAP immunostaining were prominently increased compared to CTR (Fig. 3h-k). Immunoblot analysis confirmed that Iba1 amounts were significantly higher in Tg pigs (+112%, $P < .001$ 95% CI 79–115%). Microgliosis was uniformly distributed in spinal cord, indeed no difference in protein amounts were found, considering the spinal cord level (cervical, thoracic or lumbar; $P = .871$ in thoracic and $P = .233$ in lumbar vs cervical spinal cord;) in Tg pigs (Fig. 3l). Estimates of the mean percentage differences of GFAP expression between Tg and CTR group was 94% ($P = .01$, 95% CI 22–165%) with a statistically significant increase of astrocytosis from cervical to lumbar trait in Tg compared to CTR pigs (53%, $P = .01$, 95% CI 13–159% in thoracic trait and 66%, $P = .02$, 95% CI 25–107% in the lumbar trait; Fig. 3m). In line with the activated gliosis, quantitative polymerase chain reaction analysis revealed that the proinflammatory MCP-1 mRNA levels were higher in Tg (Tg 168 and its F1 progeny, Tg 305) than those in CTR pigs (Fig. S2).

Additionally, H&E analysis of brainstem nuclei revealed vacuolization of the neurons and neuropil (Fig. 3n, o), peripheral neuronal chromatolisis (Fig. 3p), focal satellitosis and neuronophagia (Fig. 3q), in the dorsal vagal motor nucleus (DVN) and in the hypoglossal nerve nucleus (HN). In Tg but not in CTR pigs, some MNs in spinal cord ventral horn and brainstem nuclei were immunoreactive for cleaved caspase-3 (CC3), (Fig. 3r, s), however no TUNEL-positive cells were detected in CTR nor Tg pigs in the same areas (data not shown). To evaluate the autophagy pathway in the Tg168 pig, double immunofluorescence analyses of SMI32 (MN marker) and LC3 (autophagosome marker) was performed. A huge increase of LC3-positive vesicles was observed in Tg 168 pig MNs compared to CTR pig (CTR 27.95 ± 2.11 vs Tg 168 58.23 ± 2.72, $P < .001$; Fig. S3 a-h). The ultrastructure analysis of myelinated axons of the spinal cord white matter showed altered and disrupted myelin sheath, with disordered fiber arrangement and lack of mitochondria in Tg pig compared to the well-organized myelin sheath surrounding the axoplasm with healthy mitochondria, in CTR pig (Fig. S4 a-d).

3.4. Severe skeletal muscle pathology is observed in hSOD1^{G93A} Tg pigs

Gross pathologic examination of dissected muscles in symptomatic end stage Tg pigs revealed multifocal pale areas with irregular borders, widespread in many skeletal muscles especially in the tongue, diaphragm, intercostal, semimembranosus, gastrocnemius, peroneus and brachialis muscles (Fig. 4), whereas no gross muscular lesions were visible in CTR animals. Compared to age-matched CTR pigs, microscopic examination revealed severe myopathic changes consisting in a wide fiber size variability caused by hypertrophy and also atrophy, internal nuclei, myofiber necrosis, densely stained hypercontracted or basophilic regenerating fibers and proliferation of endomysial and perimysial connective tissue (Fig. 4a, b). Secondary inflammatory reaction characterized by infiltrating macrophages and lymphocytes was frequently associated with necrosis areas and phagocytosis of fibers (Fig. 4c, d). Many myofibers had also homogeneous large inclusions of pale pink material. Moreover, a few angulated atrophic fibers, ring fibers, vacuoles and rare fiber splitting were also visible (Fig. 4e-j) in symptomatic end stage Tg pigs. However, histochemical reactions for oxidative enzymes (COX, NADH-TR, SDH) did not reveal any apparent enzyme deficiency (Fig. 4e-h). Moreover, a normal distribution of glycogen was observed by PAS staining (data not shown). ATPase activity indicated that both fiber types were involved by lesions, particularly type II fibers (Fig. 4i, j). By contrast, the cytoarchitecture of extraocular

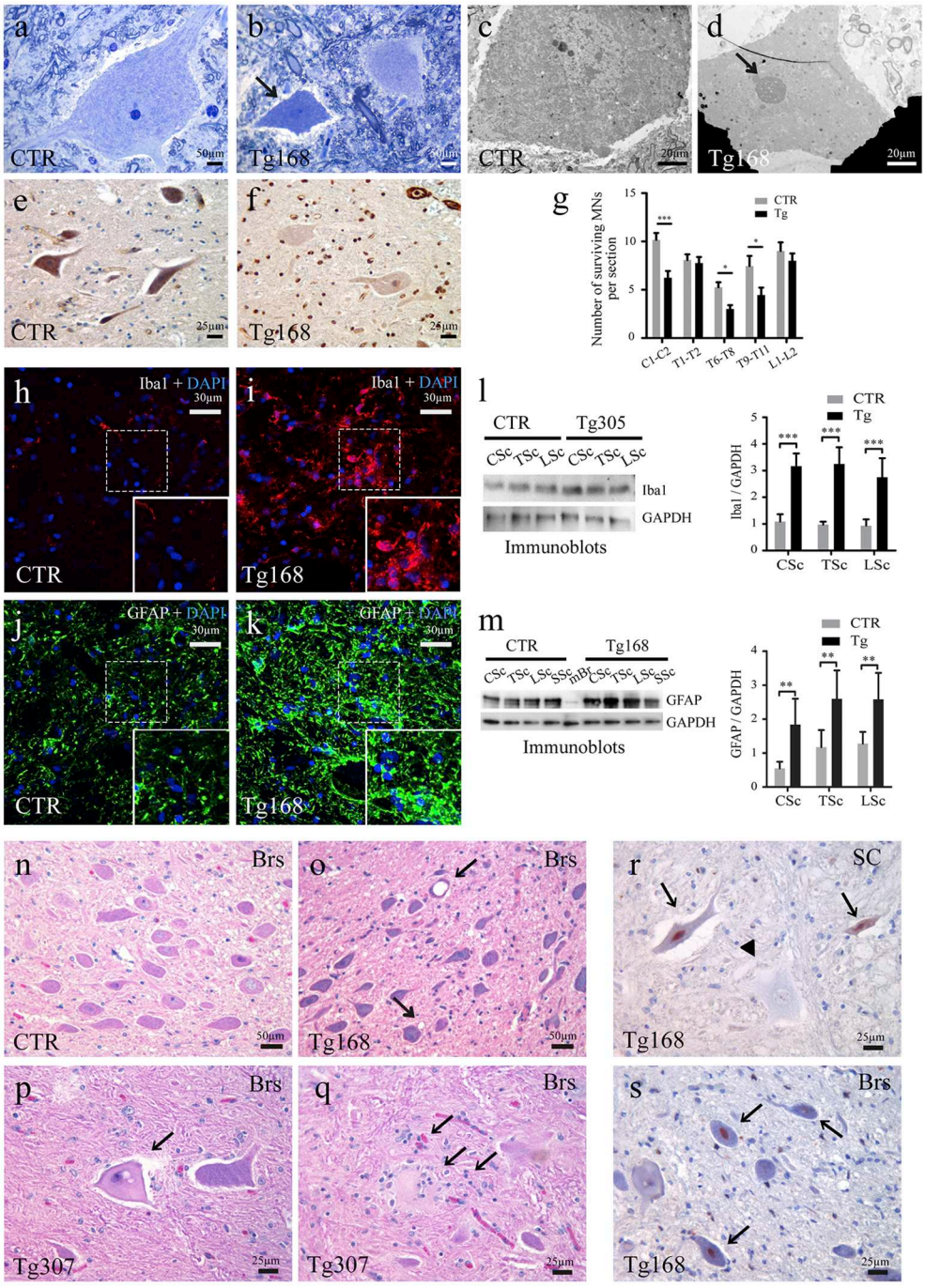

Fig. 3. MN degeneration and gliosis in end stage hSOD1^{G93A} Tg pigs spinal cord and brainstem. (a, b) Representative image of toluidine blue-stained semithin sections of lumbar spinal cord ventral horn showing degenerating motor neuron with darkened and shrunken cytoplasm in Tg pigs (arrow). (c, d) Electron microscopy image of a degenerating MN with nucleolar cavities and electron dense granules in Tg pig (arrow) as compared to CTR. (e, f) Representative immunostaining of ventral horn MNs showing normal Golgi apparatus (GA) network in CTR pig compared to fragmented GA in end stage Tg pig. (g) Quantification of surviving motor neurons from CV-stained sections showing motor neuron loss at different levels of spinal cord in end stage Tg pigs (n = 2) compared to CTR animals (n = 3). Data are mean ± s.e.m., *P < .05, ***P < .005; by univariate analysis based on multilevel mixed-effects linear regression models. (h-k) Representative images of immunostaining of lumbar spinal cord in end stage Tg versus CTR pigs for the microglial marker Iba 1 (h, i) and for the astrocytic marker GFAP (j, k). Insets highlight Iba1 and GFAP positive cells, respectively. (l, m) Representative immunoblots and quantitative analysis of Iba1 (l) and GFAP (n) proteins in cervical (CSc), thoracic (TSc), lumbar (LSc) and sacral (SSc) spinal cord samples of Tg and CTR pigs (n = 3 per group). Data are mean ± s.e.m., **P < .01, ***P < .005; by univariate analysis based on multilevel mixed-effects linear regression models. mBr; mouse brain. (n, o) Representative H&E staining image of the brainstem (Brs) showing vacuolization of motor neurons and neuropil in the dorsal vagal nerve nuclei in end stage Tg pigs (arrows). (p, q) Representative images of peripheral chromatolisis in MNs (arrow in p) and neuronophagia in the hypoglossal nerve nuclei (arrows in q) in end stage Tg animals. (r, s) Representative immunostaining of Tg spinal cord (SC) and brainstem (Brs) for the apoptotic marker cleaved caspase-3 (arrows). Arrowhead in r indicate normal healthy MN. Scale bars in μm are indicated in each photogram. (For interpretation of the references to colour in this figure legend, the reader is referred to the web version of this article.)

muscles was well preserved, as reported for human patients (data not shown). Semi-thin sections analysis from gastrocnemius muscle showed unparalleled and disarranged muscle fibers in affected Tg pigs (Fig. 4l), whereas longitudinal, regular and aligned muscle fibers with the expected typical banding pattern were detected in parallel sections of CTR pigs (Fig. 4k).

3.5. Neuromuscular junction denervation and neuropathy are evident in hSOD1^{G93A} Tg pigs

Immunofluorescence analysis of α-bungarotoxin (BTX) and neurofilament was performed and the innervation of motor endplates in gastrocnemius and peroneus muscles was scored as innervated, partially innervated or denervated (Fig. 5a-c). End stage Tg pigs showed consistent denervation of the NMJs in the gastrocnemius (24.9%) and peroneus (25.5%) muscles compared to 6.2% and 13.7% in CTR pigs (Fig. 5d). In particular, linear mixed model adjusted for muscle tissue showed a significant increase of the mean denervation percentage (15.64%, P < .0001, 95% CI 7–24.25%), in gastrocnemius (18.64%, P = .01, 95% CI 4.47–32.82%) and peroneus (11.83%; P < .0001, 95% CI 6.88–16.77%) muscles in Tg compared to CTR group. No differences were observed between Tg and CTR pigs in the percentage of partially innervated NMJs (P = .528, 95% CI 10.88–21.22%).

The morphology analysis of sciatic nerves showed uniform and compact axonal fibers in CTR pig, whereas Tg nerve exhibited differently-sized and smaller fibers, immersed in more abundant endoneurial tissue (Fig. 5e, f). The g-ratio was significantly different between CTR and Tg animals (CTR 0.498 ± 0.014 μm vs Tg 0.570 ± 0.014 μm; P = .005; Fig. 5g). Such results highlight an overall reduction in the Tg fiber size (CTR 13.3 ± 0.5 μm vs Tg 8.9 ± 0.6 μm; P = .0016),

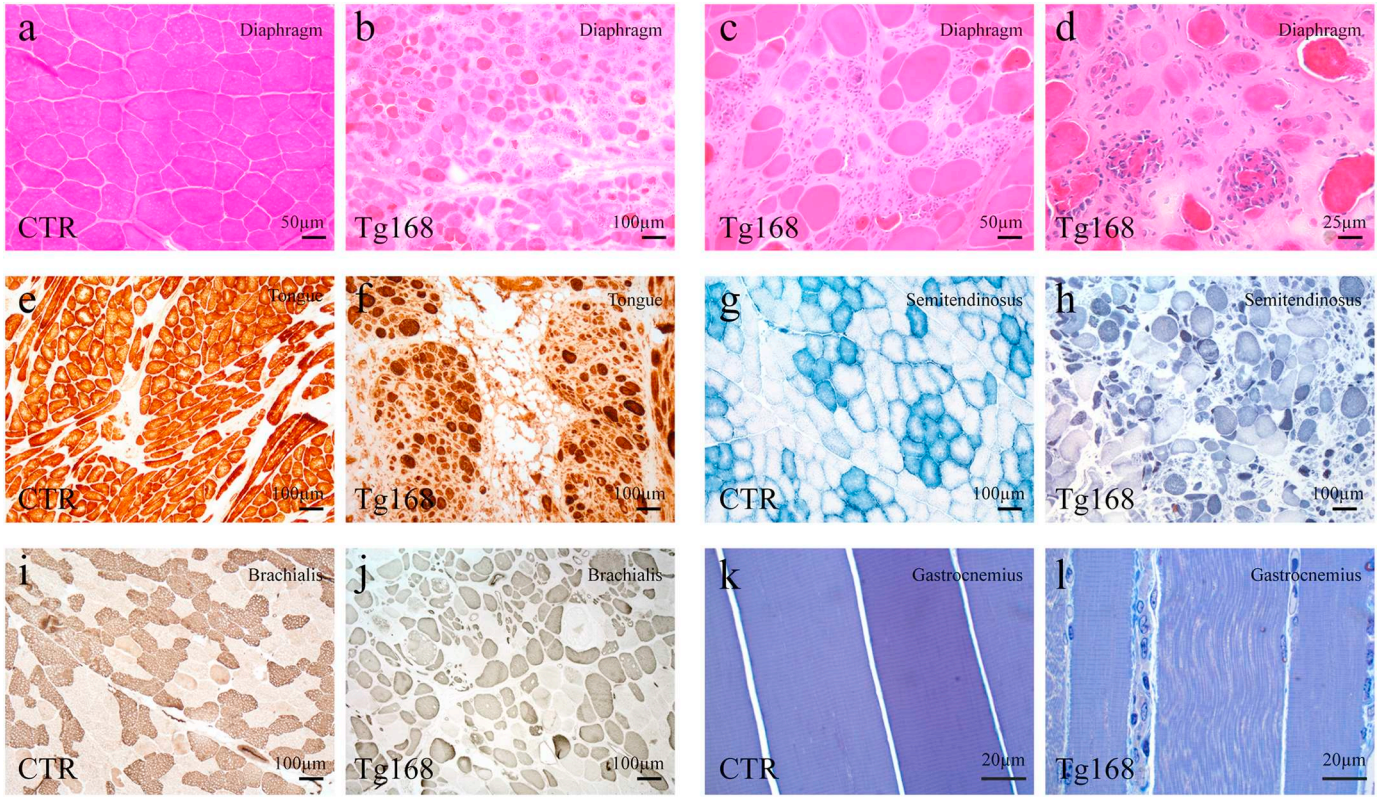

Fig. 4. Striking muscle pathology in hSOD1^{G93A} Tg pigs. (a, b) Representative images of transverse sections from CTR and Tg pigs diaphragm stained with H&E. (c, d) Higher magnification of diaphragm showing fibrosis (c) and myophagocitosis of necrotic fibers (d). (e-j) COX (e, f), NADH-TR (g, h) and ATPase (i, j) staining of intrinsic muscles of the tongue, semitendinosus and brachialis muscles respectively, in CTR and Tg pigs. (k, l) Representative image of toluidine blue-stained semithin section of gastrocnemius muscle showing unparalleled and disarranged fibers with infiltrating cells in Tg pig compared to CTR. Scale bars in µm are indicated in each photogram. (For interpretation of the references to colour in this figure legend, the reader is referred to the web version of this article.)

particularly affecting myelin thickness (CTR 6.5 ± 0.2 µm vs Tg 3.8 ± 0.3 µm; P = .0005). Moreover, the fiber size distribution revealed a remarkable shift to lower size in Tg vs CTR pigs, also underlining only in the Tg group the presence of a peak at 4–5 µm (P ≤ .001) as a plausible sign of an occurring neuropathy (Fig. 5h) (Riva et al., 2014).

3.6. hSOD1^{G93A} Tg pigs showed SOD1 aggregates and accumulation

Since cytoplasmic inclusions are a hallmark of ALS, the presence of protein aggregates was investigated. The anti-human SOD1 (hSOD1) antibody used did not recognize endogenous swine SOD1 in these experimental conditions; hSOD1 immunoreactivity was present only in Tg pigs, where it was intense in spinal cords MN cell bodies (Fig. 6a, b). In addition, hSOD1 positive skein-like and round inclusions were detected in the neuropil and within MNs both in the brainstem and spinal cord of end stage Tg pigs but not in CTRs (Fig. 6c-e). By employing a conformation-specific antibody that exclusively detects misfolded SOD1 (SEDI), the presence of positive aggregates was also demonstrated in Tg pigs (Fig. 6f). Moreover, aberrant accumulation of neurofilaments both in the Tg brainstem and spinal cord was proved by means of SMI 31 and Peripherin immunostaining (Fig. S5 a-f). Surprisingly, a prominent staining of hSOD1 in skeletal muscles was found (Fig. 6g, h). hSOD1 deposition was observed in the cytoplasm of myofibers with a scattered distribution, mainly as amorphous aggregates (Fig. 6h). By means of the SEDI antibody, the presence of misfolded hSOD1whithin these muscle aggregates was confirmed (Fig. 6i, j).

Next, SOD1 protein in the triton-insoluble fraction (TIF) as compared with the soluble fraction from both Tg versus CTR pigs, was quantified as an index of protein aggregate accumulation in different CNS areas. Notably, the amounts of the mutant hSOD1 protein were comparable to that of the endogenous swine protein (sSOD1) (linear mixed-model, P = .967) and did not vary significantly among several CNS samples (cortex, cerebellum, striatum, brainstem and spinal cord; linear mixed-model, P > .1), both in the soluble and insoluble fractions (Fig. 6k). In addition, no differences were observed between Tg and CTR pigs in the levels of endogenous sSOD1 protein (linear mixed-model, P = .127). Comparing the levels of soluble and triton-insoluble protein, the last was higher in Tg pigs, though it was not statistically significant (linear mixed-model, P > .1).

3.7. TDP-43 levels in PBMCs as a potential biomarker for disease onset

The increase of the TDP-43 protein level in PBMCs parallels the disease progression in ALS patients (Nardo et al., 2011). Therefore this biomarker was investigated in symptomatic, asymptomatic hSOD1^{G93A} Tg pigs and also in CTR pigs. TDP-43 levels were low and comparable between CTR and Tg pigs that did not develop the disease (Tg 174, 204, 205). In PBMC samples of presymptomatic pigs (Tg 409, Tg 411 and Tg 168), TDP-43 levels were significantly higher than CTR pigs (P < .05). In particular, in PBMC samples of Tg 168 pig, the TDP-43 began to raise during the very early presymptomatic stage (from 22 to 25 months of age), doubled its level at 25 months of age compared with the asymptomatic and CTR samples, and reached the highest level when the disease was at the end stage (P < 0,05 versus CTR, asympptomatic and presymptomstic pigs). In conclusion, the TDP-43 levels raised at least two months before the onset of the clinical symptoms, opening the possibility to employ this biomarker to monitor the ALS families even at presymptomatic stage (Fig. 7). In addition, to further characterize TDP-43 pathology in the Tg swine model, insoluble TDP-43 in spinal cord and frontal cortex tissues of Tg pigs (Tg 168, 305, 307) and CTRs, was measured. As shown in Fig. S6 a, b, the level of TDP-43 in the TIF

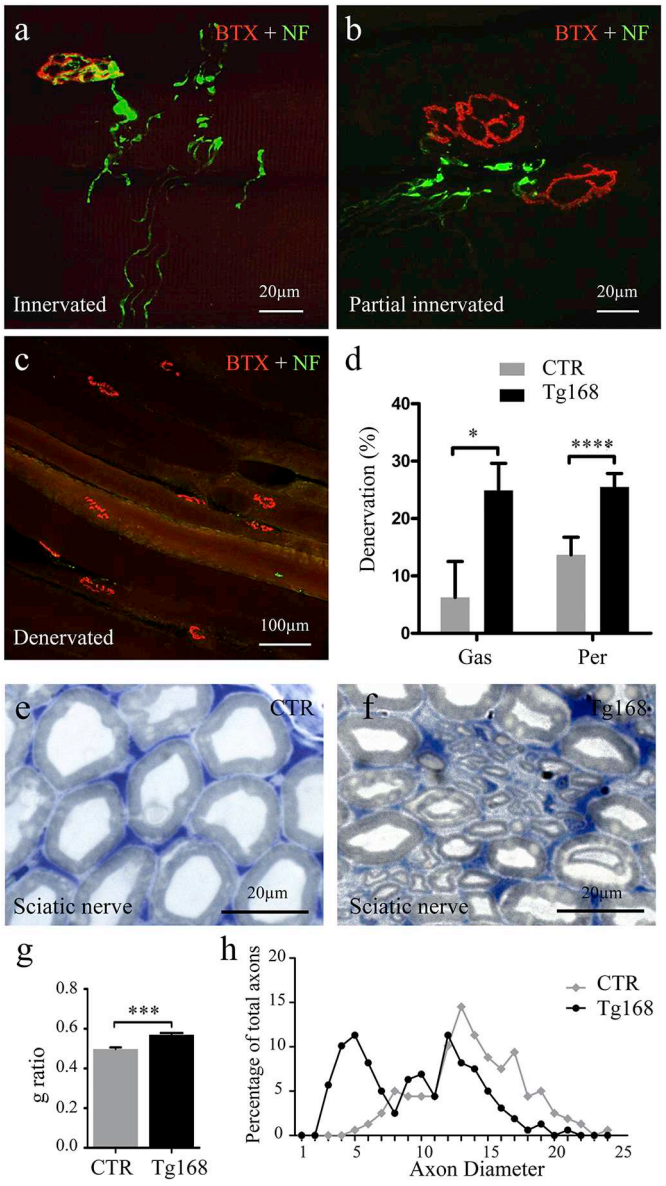

Fig. 5. Tg hSOD1^{G93A} pigs show signs of muscle denervation and peripheral axonopathy. (a-c) Representative images of neuromuscular junctions (red), acetylcholine receptor labeled with α- bungarotoxin (BTX), and motor axons labeled with anti-neurofilament (NF) antibody (green) considered as innervated, partially innervated and denervated. (d) Quantification of the percentage of denervation in gastrocnemius and peroneus muscle. Count was performed in at least 100 NMJs per muscle. Data are mean ± s.e.m., *P < .05, ****P < .0001; by univariate analysis based on multilevel mixed-effects linear regression models. (e-f) Representative image of toluidine-blue stained sciatic nerve semithin sections in CTR as compared to Tg pigs. (g) Graph depict the g-ratio quantification of sciatic nerve fibers in Tg and CTR pigs (n = 3 per group). Data are mean ± s.e.m., ***P < .005; unpaired *t*-test. (h) Axon size distribution in sciatic nerve from CTR and Tg pigs. Scale bars in μm are indicated in each photogram. (For interpretation of the references to colour in this figure legend, the reader is referred to the web version of this article.)

fraction was higher in Tg than in CTR pigs, although *t*-test was not significant (P = .1 for spinal cord and P = .07 for frontal cortex). Interestingly, increased levels of insoluble TDP-43 with the same method were found also in G93ASOD1 mouse models of ALS (Lauranzano et al., 2015; Marino et al., 2015). Moreover, in cervical spinal cord the levels of nuclear and cytoplasmic TDP-43 were respectively lower and higher in Tg 168 than CTR pig (Fig. S7 a, b), indicative of a cytoplasmic mislocalization of TDP-43, similarly to the G93ASOD1 mouse model (Lauranzano et al., 2015). Consistently, weaker nuclear TDP-43 staining of large neurons was found in Tg 168 compared to CTR pig, even if no TDP-43-positive cytoplasmic inclusions were apparent (Fig. S7 c, d). Nevertheless, the affected SMI-31-positive MN in Tg pigs were TDP 43 and phospho TDP-43 positive as observed in serial sections (Fig. S7 e-g).

4. Discussion

In this study, a swine model of familial ALS disease is described. The expression of the human pathological allele of SOD1 gene with the G93A mutation caused an ALS like-disease in pigs with an autosomal mendelian trait. As in humans, the onset of the ALS disease occurs after a quite long asymptomatic period (about 27 months) with full penetrance in the progeny of affected transgenic pigs.

According to what reported for ALS mouse models expressing pathological human SOD1 alleles, transgene copy number and expression level of the pathological protein are critical factors to determine the severity of the disease (Alexander et al., 2004). Four swine founders were initially investigated; the Tg 168 founder developed ALS-like disease at 27 months of age, while the others, Tg 174, Tg 204 and Tg 205 (Tg 204-clone) that have lower transgene copy number and low amount of hSOD1^{G93A} protein, did not develop the clinical phenotype up to 5 years of age. It cannot be excluded that the latter founders might develop similar signs and symptoms later, however genetic background, epigenetic effects on the transgenic integration site, DNA rearrangements or other molecular events may occur and further investigations are required.

Tg 168 founder developed a neuromuscular disease characterized by progressive paresis, MN degeneration and gliosis. Cytogenetic and molecular analysis revealed that the transgenic vector was integrated in multiple (about 20 copies) tandem-repeat copies in a single site of the host swine genome on chromosome 2q24. High resolution mapping allowed to map the chromosome breakpoint at `chr2: bp124045533` quite far (about 655 kb and 288 kb at the 5′ and 3′ end of the breakpoint, respectively) from known coding genes, supporting the evidence that no coding genes were interrupted by the integration event. This is also evident from the genotype analysis of the Tg 168 progeny. Indeed, the disease is transmitted as an autosomal mendelian trait and the homozygous Tg 559 pig was born alive and developed the disease earlier at about 12 months of age. A threshold level of pathological hSOD1^{G93A} seems to be required to trigger the disease by a gain of function mechanisms, however immunoblot analysis showed comparable amounts between transgenic and endogenous SOD1 proteins, which may reasonable exclude any putative aspecific toxic or artificial effect due to overexpression of the transgenic protein, such as squelching, on causing the clinical symptoms. Another transgenic SOD1^{G93A} pig model was reported by Yang et al. (Yang et al., 2014) showing hSOD1 expression level lower than or equivalent to the endogenous one; however, in these pigs limb movement defects started as early as 3 months of age. This discrepancy could be dependent on several factors widely explored in SOD1 mice (i.e. gender, genetic background); moreover, no transgene integration data were reported for this model.

From a clinical point of view, Tg pigs showed a long pre-symptomatic phase lasting about two years followed by the development of gait abnormality starting on hind limbs and which progressively worsened with concomitant dysphagia and severe respiratory impairment, till the humane end point was reached, after approximately four months. Similarly, in humans, the mutant G93A SOD1 is associated to a rapid disease progression and more severe neurological symptoms which last 1 to, at most, 4 years (Kato, 2008); moreover, SOD1 patients present mostly with limb onset, starting predominantly in lower limb rather than upper limb. Those cases with worse prognosis present also with bulbar onset with dysarthria, dysphagia and earlier respiratory dysfunction due to involvement of the cervical phrenic MNs (Chen

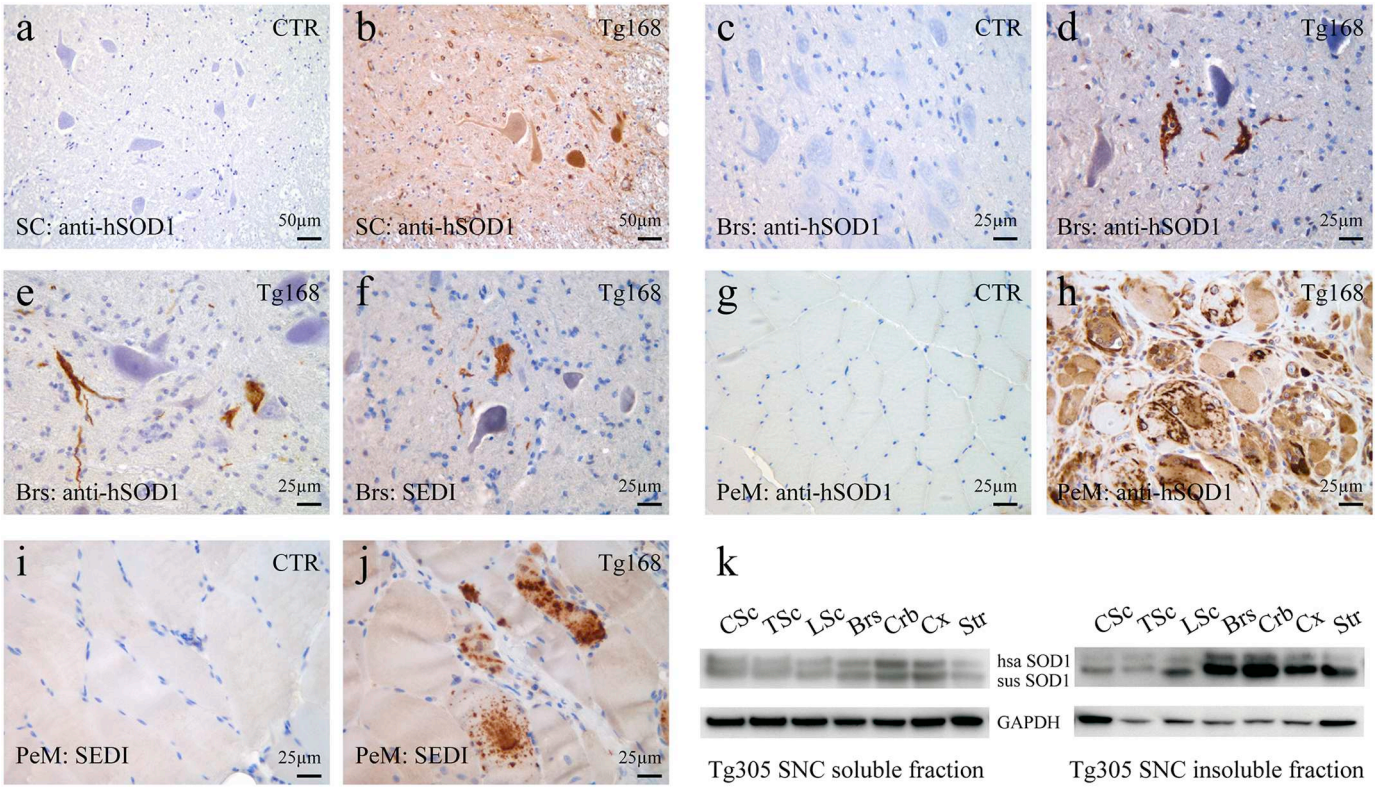

Fig. 6. Mutant SOD1 protein aggregates in hSOD1^{G93A} Tg pigs. (a-d) Representative images of spinal cord ventral horn (a, b) and brainstem motor nuclei (c, d) revealing intense immunostaining for hSOD1 in motor neurons cell bodies in Tg but not in CTR pigs. (e) Representative image of filamentous and skein-like aggregates of hSOD1 in brainstem of Tg pigs. (f) Representative images of immunostaining for misfolded hSOD1 (SEDI antibody) in brainstem of Tg pigs. (g-j) Representative images of immunostaining of peroneus muscle (PeM) in end stage Tg versus CTR pigs showing intense staining for hSOD1 (g, h) and the presence of aggregates SEDI positive within the fibers (i, j). (k) Representative immunoblot of hSOD1 detected in soluble and triton-insoluble fractions in end stage Tg pig brain and spinal cord. SC: spinal cord; Brs: brainstem; C: cervical; T: thoracic; L: lumbar; Crb: cerebellum; Cx: cerebral cortex; Str: striatum; hsa: human; sus: porcine. Scale bars in µm are indicated in each photogram.

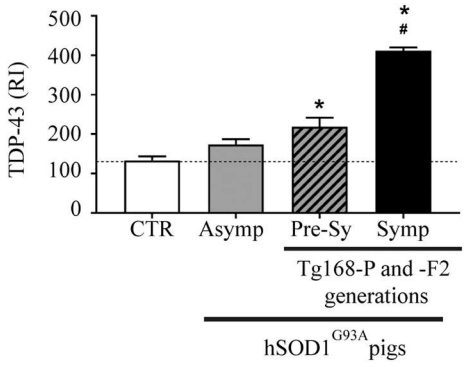

Fig. 7. Total TDP-43 protein levels were analyzed by dot blot analysis in PBMC samples isolated from CTR pigs (C1, C2, 310), Tg founder pigs that did not develop the disease (Asymp: Tg 204, Tg 205, Tg 174) and Tg pigs that developed the disease at a presymptomatic (Tg 409, Tg 411, Tg 168) and a symptomatic (Tg 168) stage. CTR (C1: n = 10; C2: n = 15; 310: n = 6), Asymp (204: n = 12, 205: n = 12: 174: n = 12), Presymp (409: n = 3; 411: n = 2, 168: n = 4) and Symp (Tg168: n = 3). Data are mean ± s.e.m., of the levels measured at different time points. Asymptomatic Tg pigs (204, 205, 174) were analyzed from 22 to 44 months of age. Immunoreactivity was normalized to protein loading, as assessed by Ponceau Red staining (Relative Immunoreactivity, RI). *P < .05 versus CTRs, #P < .05 versus Asymp and Presymp, by one-way ANOVA, Tukey's multiple comparisons test.

et al., 2013; Swinnen and Robberecht, 2014) underlying that the clinical phenotype in Tg pigs resembled that of ALS patients. In order to both test muscle activity during gait in awake pigs and to reduce the invasiveness of the procedure, electrophysiological analysis by sEMG instead of needle EMG, was performed. A clear pattern of spastic co-contraction of the gastrocnemius and peroneus muscle in Tg 168 at the end stage but not in control pigs or other asymptomatic Tg pigs was observed. Spasticity is reported in patients as a sign of upper motor neuron involvement; here, the motor cortex role is under investigation.

At disease end-stage, Tg pigs developed key neuropathological features of ALS including MNs degeneration and loss, gliosis and the presence of SOD1 positive inclusions. In particular, the number of surviving MNs was decreased in Tg pigs compared to control pigs in some areas of the spinal cord, confirming the focal spread of the disease as observed in patients (Ravits and La Spada, 2009), whereas activated astrocytes and microglia were increased in association with an increase of the proinflammatory chemokine MCP-1 which has been demonstrated to correlate with the disease progression in ALS patient and mouse model (Guo et al., 2017; Kawaguchi-Niida et al., 2013). Additionally, Tg pig showed shrunken and atrophied neuronal cell bodies with nucleolar alterations. Similar abnormalities were reported as a sign of degeneration preceding neuronal death (Kiernan and Hudson, 1993) and analogous nucleolar enlargement have been described in a murine model of Pukinje cell degeneration (Baltanas et al., 2011). Moreover, although vacuolization pathology is not a common feature in postmortem tissues of both sporadic ALS (SALS) and familial (FALS) patients at the end stage (Higgins et al., 2003), SOD1 mice exhibit abundant vacuoles in neurons and neuropil at the presymptomatic stage of disease which become less evident at the end stage (Bendotti et al., 2012; Sumi et al., 2006). Thus, the mild vacuolization pathology observed in the brainstem of Tg pigs may represent an early stage in the process of neurodegeneration. Another interesting result obtained in Tg

pigs is the presence of MNs Cleaved Caspase 3, a final effector of apoptotic cell death, but none TUNEL-positive cells. Even if there is compelling evidence indicating that MN death in ALS patients and $SOD1^{G93A}$ mice does not occur through apoptosis (He and Strong, 2000; Migheli et al., 1999), a toxic cascade characterized by the sequential activation of Caspase 1 and Caspase 3 has been implicated in the vulnerability of MNs in ALS (Pasinelli et al., 2000). Our results in Tg pigs confirm previous findings in ALS mice, suggesting that caspase activation is a feature of neurodegenerative processes associated to mutant SOD1 but MN death do not occur through apoptosis. The evaluation of the autophagy pathway revealed a huge increase in the number of LC3-positive vesicles in Tg ventral horn MNs suggesting a likely dysfunction of the autophagic system in Tg swine model; a similar upregulation of autophagic markers has been already reported in several ALS murine models and in human patients (Nguyen et al., 2018; Song et al., 2012). Tg pigs showed loss of the normal network of elements of the Golgi Apparatus (GA), which appeared dispersed and isolated in most of the remaining spinal MNs. The fragmentation of the GA was frequently observed in patients with sporadic, familial and juvenile ALS and in $SOD1^{G93A}$ Tg mice appears long before the onset of disease suggesting that it is an early sign of neuronal degeneration (Fujita and Okamoto, 2005). Moreover, it was suggested that GA fragmentation could be related to the presence of protein aggregates which were detected in our Tg pigs, contrary to that was previously reported in a similar hSOD1 pig model (Yang et al., 2014). Protein aggregates represent a hallmark of ALS in humans, appearing as intracytoplasmic eosinophilic inclusions (Bunina bodies) or as round ialine and skein like inclusions (Blokhuis et al., 2013). In brainstem neurons and neuropil of our Tg pigs we found both round and skein-like inclusions which were immunopositive for hSOD1 and most importantly, for the misfolded form of SOD1. Therefore, altogether these data suggest the validity of Tg pigs as a useful model to study certain etiopathogenetic aspects (e.g. protein misfolding and aggregation) in ALS.

Particularly striking in our Tg pig model is the muscular pathology characterized by necrosis and inflammation associated to a massive deposition of the human SOD1 protein, NMJ denervation and distal axonopathy. Acute or chronic neurogenic atrophy and mitochondria dysfunction are common findings in muscle biopsies of FALS and SALS patients and similarly Tg SOD1 mice. Our results in Tg pigs at the end stage revealed a pattern resembling a muscular dystrophy rather than a mere denervation atrophy with the presence of several degrees of inflammation, necrosis and fibrosis. This severe muscular pathology could be due to the elevated expression of mutant SOD1 in skeletal muscles of our Tg pigs. Wong et al. (Wong and Martin, 2010) demonstrated that hSOD1 toxicity to skeletal muscles involves oxidative damage and nitrative stress but it is independent of the formation of SOD1 aggregates. Nevertheless, the role of mutant SOD1 aggregates in impairing protein conformation and the consequent muscle loss in ALS remains elusive (Wei et al., 2012). To our knowledge, there are no reports regarding SOD1 aggregation in ALS patient muscles, however, the presence of dystrophic-like changes in Tg pigs suggests that mutant SOD1 might contributes to muscle degeneration. Substantial evidence indicates that the pathological process leading to ALS involves multiple cell types, including skeletal muscle cells. In particular, different studies demonstrated in both ALS patients and animal models, defects in the skeletal muscle that occur even in the absence of motor neuron death, supporting the “dying-back” hypothesis in which distal motor endplate degeneration plays a key role in the progression of the disease (Dupuis and Loeffler, 2009; Fischer et al., 2004; Musaro, 2013; Rocha et al., 2013). Selective expression of mutant SOD1 in mouse skeletal muscles under the transcriptional control of muscle-specific promoter (MLC) induced progressive muscle atrophy, reduction in muscle strength and mitochondrial dysfunction without MN degeneration (Dobrowolny et al., 2008). On the contrary, another study reported that the expression of mutant SOD1 in skeletal muscles causes MN degeneration as a later event after muscle pathology (Wong and Martin, 2010). Thus, although initially the “neurocentric” dogma assumed that MN degeneration, caused by mutant SOD1, was the main driver of muscular atrophy, more recent evidence suggests that muscular dysfunction could precede and contribute in triggering MN degeneration (Fischer et al., 2004; Frey et al., 2000; Moloney et al., 2014). Consistently, we found that Tg pigs displayed marked signs of distal axonopathy and denervation in the gastrocnemius and peroneus muscles despite of the lack of a significant loss of MNs in the lumbar spinal cord. Further studies involving animals at different stage of disease (e.g. early, mid and late symptomatic) are requested.

Notably, we have also found that Tg pigs that develop the disease has a higher total TDP-43 protein level in PBMCs than CTR and asymptomatic Tg controls, similarly to ALS patients (Filareti et al., 2017; Nardo et al., 2011) thus confirming the robustness of the pathological phenotype of this animal model. Moreover, we demonstrated that total TDP-43 protein level is an early disease biomarker, since it underscores disease also before overt clinical symptoms, an aspect that could not be explored in the patients. Interestingly, in this respect the Tg pig model is more similar to the patients than to the $SOD1^{G93A}$ mouse model in which we could not find higher TDP-43 levels in PBMCs compared to CTRs (Filareti et al., 2017).

In conclusion, altogether our data demonstrated that Tg pigs might represent a similar and representative model of human ALS and thus offer several advantages compared to rodents such as the possibility to study the etiopathogenetic events that precede the onset of disease and potential diagnostic and prognostic biomarkers. Furthermore, the longer symptomatic phase and the large size might allow to test for novel drugs and possible advanced therapy medicinal products.

Supplementary data to this article can be found online at https://doi.org/10.1016/j.nbd.2018.11.021.

Conflicts of interest

The authors declare that they have no competing interests.

Acknowledgments

We would like to thank R. Maritano (Department of Veterinary Sciences, University of Turin) for animal care; Silvia Luotti e Melania Filareti (Mario Negri) for help in biomarker analysis; Simone Bompasso (Neuroscience Institute Cavalieri Ottolenghi, Department of Clinical and Biological Sciences, University of Turin) for the assistance in electron microscopy sample preparation. This work was supported by funding from Italian Ministry of Health (GR-2010-2312522 to C. Corona; 15CEA and 16CEA to C. Casalone) and Compagnia di San Paolo Foundation (ROL15198) to C. Casalone, by Programma Nazionale per la Ricerca-CNR “Aging Program 2012- 2014” to P.V., by Superpig project co-financed by Lombardy Region through the Fund for Promoting Institutional Agreements, by Fondazione Avantea to C.G.

References

Alexander, G.M., et al., 2004. Effect of transgene copy number on survival in the G93A SOD1 transgenic mouse model of ALS. Brain Res. Mol. Brain Res. 130, 7–15.
Andersen, P.M., 2006. Amyotrophic lateral sclerosis associated with mutations in the CuZn superoxide dismutase gene. Curr. Neurol. Neurosci. Rep. 6, 37–46.
Baltanas, F.C., et al., 2011. Purkinje cell degeneration in pcd mice reveals large scale chromatin reorganization and gene silencing linked to defective DNA repair. J. Biol. Chem. 286, 28287–28302.
Basso, M., et al., 2009. Characterization of detergent-insoluble proteins in ALS indicates a causal link between nitrative stress and aggregation in pathogenesis. PLoS One 4, e8130.
Benatar, M., 2007. Lost in translation: treatment trials in the SOD1 mouse and in human ALS. Neurobiol. Dis. 26, 1–13.
Bendotti, C., et al., 2012. Dysfunction of constitutive and inducible ubiquitin-proteasome system in amyotrophic lateral sclerosis: implication for protein aggregation and immune response. Prog. Neurobiol. 97, 101–126.
Blokhuis, A.M., et al., 2013. Protein aggregation in amyotrophic lateral sclerosis. Acta Neuropathol. 125, 777–794.
Chen, S., et al., 2013. Genetics of amyotrophic lateral sclerosis: an update. Mol.

Neurodegener. 8, 28.
Chieppa, M.N., et al., 2014. Modeling amyotrophic lateral sclerosis in hSOD1 transgenic swine. Neurodegener. Dis. 13, 246–254.
Courtine, G., et al., 2005. Kinematic and EMG determinants in quadrupedal locomotion of a non-human primate (Rhesus). J. Neurophysiol. 93, 3127–3145.
Dobrowolny, G., et al., 2008. Skeletal muscle is a primary target of SOD1G93A-mediated toxicity. Cell Metab. 8, 425–436.
Dupuis, L., Loeffler, J.P., 2009. Neuromuscular junction destruction during amyotrophic lateral sclerosis: insights from transgenic models. Curr. Opin. Pharmacol. 9, 341–346.
Eisen, A., 2014. Response to a letter by Dr T Ramesh. J. Neurol. Neurosurg. Psychiatry 85, 1289.
Filareti, M., et al., 2017. Decreased levels of foldase and chaperone proteins are associated with an early-onset amyotrophic lateral sclerosis. Front. Mol. Neurosci. 10, 99.
Fischer, L.R., et al., 2004. Amyotrophic lateral sclerosis is a distal axonopathy: evidence in mice and man. Exp. Neurol. 185, 232–240.
Frey, D., et al., 2000. Early and selective loss of neuromuscular synapse subtypes with low sprouting competence in motoneuron diseases. J. Neurosci. 20, 2534–2542.
Fujita, Y., Okamoto, K., 2005. Golgi apparatus of the motor neurons in patients with amyotrophic lateral sclerosis and in mice models of amyotrophic lateral sclerosis. Neuropathology 25, 388–394.
Guo, J., et al., 2017. Evaluating the levels of CSF and serum factors in ALS. Brain Behav. 7, e00637.
He, B.P., Strong, M.J., 2000. Motor neuronal death in sporadic amyotrophic lateral sclerosis (ALS) is not apoptotic. A comparative study of ALS and chronic aluminium chloride neurotoxicity in New Zealand white rabbits. Neuropathol. Appl. Neurobiol. 26, 150–160.
Higgins, C.M., et al., 2003. ALS-associated mutant SOD1G93A causes mitochondrial vacuolation by expansion of the intermembrane space and by involvement of SOD1 aggregation and peroxisomes. BMC Neurosci. 4, 16.
Holm, I.E., et al., 2016. Genetically modified pig models for neurodegenerative disorders. J. Pathol. 238, 267–287.
Kato, S., 2008. Amyotrophic lateral sclerosis models and human neuropathology: similarities and differences. Acta Neuropathol. 115, 97–114.
Kawaguchi-Niida, M., et al., 2013. MCP-1/CCR2 signaling-mediated astrocytosis is accelerated in a transgenic mouse model of SOD1-mutated familial ALS. Acta Neuropathol. Commun. 1, 21.
Kiernan, J.A., Hudson, A.J., 1993. Changes in shapes of surviving motor neurons in amyotrophic lateral sclerosis. Brain 116 (Pt 1), 203–215.
Lauranzano, E., et al., 2015. Peptidylprolyl isomerase A governs TARDBP function and assembly in heterogeneous nuclear ribonucleoprotein complexes. Brain 138, 974–991.
Lind, N.M., et al., 2007. The use of pigs in neuroscience: modeling brain disorders. Neurosci. Biobehav. Rev. 31, 728–751.
Marino, M., et al., 2015. Differences in protein quality control correlate with phenotype variability in 2 mouse models of familial amyotrophic lateral sclerosis. Neurobiol. Aging 36, 492–504.
Migheli, A., et al., 1999. Lack of apoptosis in mice with ALS. Nat. Med. 5, 966–967.
Moloney, E.B., et al., 2014. ALS as a distal axonopathy: molecular mechanisms affecting neuromuscular junction stability in the presymptomatic stages of the disease. Front. Neurosci. 8, 252.
Musaro, A., 2013. Understanding ALS: new therapeutic approaches. FEBS J. 280, 4315–4322.
Nardo, G., et al., 2011. Amyotrophic lateral sclerosis multiprotein biomarkers in peripheral blood mononuclear cells. PLoS One 6, e25545.
Neumann, M., 2009. Molecular neuropathology of TDP-43 proteinopathies. Int. J. Mol. Sci. 10, 232–246.
Nguyen, D.K.H., et al., 2018 Apr 4. Autophagy as a common pathway in amyotrophic lateral sclerosis. Neurosci. Lett. https://doi.org/10.1016/j.neulet.2018.04.006. pii: S0304-3940(18)30261-1 (Epub ahead of print).
Ouyang, Y.B., Hu, B.R., 2001. Protein ubiquitination in rat brain following hypoglycemic coma. Neurosci. Lett. 298, 159–162.
Pasetto, L., et al., 2017. Targeting extracellular cyclophilin A reduces neuroinflammation and extends survival in a mouse model of amyotrophic lateral sclerosis. J. Neurosci. 37, 1413–1427.
Pasinelli, P., et al., 2000. Caspase-1 and -3 are sequentially activated in motor neuron death in Cu, Zn superoxide dismutase-mediated familial amyotrophic lateral sclerosis. Proc. Natl. Acad. Sci. U. S. A. 97, 13901–13906.
Paulis, M., et al., 2015. A pre-screening FISH-based method to detect CRISPR/Cas9 off-targets in mouse embryonic stem cells. Sci. Rep. 5, 12327.
Perrin, S., 2014. Preclinical research: make mouse studies work. Nature 507, 423–425.
Peviani, M., et al., 2010. Unraveling the complexity of amyotrophic lateral sclerosis: recent advances from the transgenic mutant SOD1 mice. CNS Neurol. Disord. Drug Targets 9, 491–503.
Potter, C.J., Luo, L., 2010. Splinkerette PCR for mapping transposable elements in Drosophila. PLoS One 5, e10168.
Ravits, J.M., La Spada, A.R., 2009. ALS motor phenotype heterogeneity, focality, and spread: deconstructing motor neuron degeneration. Neurology 73, 805–811.
Riva, N., et al., 2014. Balance exercise in patients with chronic sensory ataxic neuropathy: a pilot study. J. Peripher. Nerv. Syst. 19, 145–151.
Rocha, M.C., et al., 2013. Early changes of neuromuscular transmission in the SOD1(G93A) mice model of ALS start long before motor symptoms onset. PLoS One 8, e73846.
Rosen, D.R., 1993. Mutations in Cu/Zn superoxide dismutase gene are associated with familial amyotrophic lateral sclerosis. Nature 364, 362.
Song, C.Y., et al., 2012. Autophagy and its Comprehensive Impact on ALS. Int. J. Neurosci. 122, 695–703.
Sumi, H., et al., 2006. Inverse correlation between the formation of mitochondria-derived vacuoles and Lewy-body-like hyaline inclusions in G93A superoxide-dismutase-transgenic mice. Acta Neuropathol. 112, 52–63.
Sumi, H., et al., 2009. Nuclear TAR DNA binding protein 43 expression in spinal cord neurons correlates with the clinical course in amyotrophic lateral sclerosis. J. Neuropathol. Exp. Neurol. 68, 37–47.
Swinnen, B., Robberecht, W., 2014. The phenotypic variability of amyotrophic lateral sclerosis. Nat. Rev. Neurol. 10, 661–670.
Talbot, K., 2014. Amyotrophic lateral sclerosis: cell vulnerability or system vulnerability? J. Anat. 224, 45–51.
Thorup, V.M., et al., 2008. Net joint kinetics in the limbs of pigs walking on concrete floor in dry and contaminated conditions. J. Anim. Sci. 86, 992–998.
Turner, B.J., Talbot, K., 2008. Transgenics, toxicity and therapeutics in rodent models of mutant SOD1-mediated familial ALS. Prog. Neurobiol. 85, 94–134.
Wei, R., et al., 2012. Protein misfolding, mitochondrial dysfunction and muscle loss are not directly dependent on soluble and aggregation state of mSOD1 protein in skeletal muscle of ALS. Biochem. Biophys. Res. Commun. 417, 1275–1279.
Wong, M., Martin, L.J., 2010. Skeletal muscle-restricted expression of human SOD1 causes motor neuron degeneration in transgenic mice. Hum. Mol. Genet. 19, 2284–2302.
Yang, H., et al., 2014. Species-dependent neuropathology in transgenic SOD1 pigs. Cell Res. 24, 464–481.